

On the Effect of Pipe Boundary Layer Growth on the Formation of a Laminar Vortex Ring Generated by a Piston/Cylinder Arrangement

Michael Shusser and Morteza Gharib

Graduate Aeronautical Laboratories,
California Institute of Technology,
Pasadena, CA 91125, U.S.A.

Moshe Rosenfeld

Faculty of Engineering, Tel Aviv University,
Tel Aviv 69978, Israel

Kamran Mohseni

Department of Aerospace Engineering Sciences,
University of Colorado,
Boulder, CO 80309-0429, U.S.A.

Communicated by R.D. Moser

Received 19 January 2000 and accepted 17 August 2001

Abstract. The growth of a boundary layer at the nozzle wall during laminar vortex ring formation by a nozzle flow generator (piston/cylinder arrangement) is analysed theoretically and numerically and used for modelling the formation of real vortex rings. The predictions of the model are in good agreement with previous experimental and numerical results.

1. Introduction

Vortex rings are usually generated in the laboratory by the motion of a piston pushing a column of fluid of length L through an orifice or nozzle of diameter D . This results in a separation of the boundary layer at the edge of the orifice or nozzle and its subsequent spiral roll-up.

The piston/cylinder arrangement has been extensively used to address the problem of vortex ring formation (Shariff and Leonard, 1992; Lim and Nickels, 1995). Recently Gharib *et al.* (1998) in their experimental study of vortex ring formation addressed the question of the largest circulation that a vortex ring can attain, by increasing L/D while keeping the average piston velocity fixed.

Gharib *et al.* (1998) showed that two distinct states of the flow exist for a wide range of the ratio of piston-stroke-to-diameter (L/D) or “formation times”. Whereas for small stroke ratios only a single vortex ring was observed, the flow-field generated by large L/D values always resulted in a leading vortex ring followed by

a trailing jet. Comparing the total circulation produced by the motion of the piston with that of the resulting vortex ring, they were able to define the time of the transition between these two flow states, i.e. when the vortex ring pinches off from its generating axisymmetric jet.

It turned out that the pinch-off was always observed to occur at a stroke ratio (formation time) of approximately 4. This universal time scale was called the “formation number”. The universality of this number was tested by generating vortex rings with different jet exit diameters, Reynolds numbers and exit boundary conditions, as well as with various non-impulsive piston velocities programs.

The existence of the formation number was shown to be consistent with the Kelvin–Benjamin variational principle for steady axis-touching vortex rings (Kelvin, 1880, Section 18; Benjamin, 1976). According to this principle, a steady translating vortex ring has maximum energy with respect to impulse-preserving iso-vortical (i.e. preserving the circulation of each fluid element) perturbations. It has been used in the mathematical literature for investigating stability and existence of vortex-ring-type solutions (Friedman and Turkington, 1981; Amick and Fraenkel, 1986; Wan 1988). It follows from this principle that the pinch-off occurs when the apparatus is no longer able to deliver the energy required for the existence of a steady vortex ring. Gharib *et al.* (1998) demonstrated that based on the measured impulse, circulation and energy of the observed vortex rings, the Kelvin–Benjamin variation principle correctly predicts the range of the observed formation numbers.

Mohseni and Gharib (1998) used this idea to predict the formation number analytically by considering the dimensionless energy of a vortex ring. It follows from their analysis that the translational velocity of the ring $W = 0.5 U_P$, where U_P is the piston velocity. The predictions of the model were in reasonable agreement with experiment, though the authors mention that in practice the translational velocity of a vortex ring is higher.

Mohseni (2001) offered a statistical equilibrium theory for the vortex ring pinch-off process. He found that the final equilibrium state predicted by mixing entropy maximization in statistical equilibrium theory satisfies an energy extremization similar to the Kelvin–Benjamin variational principle.

Rosenfeld *et al.* (1998) extended the experimental study of Gharib *et al.* (1998) by investigating numerically the formation of a laminar vortex ring. Utilizing computational fluid dynamics techniques, the authors were able to study the influence of parameters, such as the velocity profile of the ring-generating discharging jet, that are almost impossible to investigate experimentally. The authors considered separately the case of a specified velocity profile and the general case of piston/cylinder arrangement.

Rosenfeld *et al.* (1998) showed that the formation number is strongly dependent on the velocity profile and also, though to a lesser extent, depends on the velocity program (the piston velocity as a function of time). The latter observation was also made by Gharib *et al.* (1998) who in their experiments obtained that the formation number lies in the range of 3.8–4.2 for an impulsive velocity program (constant piston velocity) but can be as large as 4.5 for time-dependent velocity programs.

Recently, Mohseni *et al.* (2001) considered numerical simulation of vortex ring formation by applying a non-conservative force of long duration. This was offered as a model for vortex generation in a piston/cylinder mechanism. They observed that the leading vortex ring pinches off with normalized energy and circulation of about 0.3 and 2.0, respectively, consistent with the theoretical predictions of Gharib *et al.* (1998) and Mohseni and Gharib (1998). These two non-dimensional parameters are formed with three integrals of the motion (energy, circulation and impulse) and the translational velocity of the leading vortex ring. They showed that by increasing the nozzle diameter or accelerating piston velocity during the formation process, thicker rings (similar to Hill’s spherical vortex) with larger normalized circulation can be generated.

The interaction of the trailing jet instability with the leading vortex ring was studied recently by Zhao *et al.* (2000). While their numerical simulation confirms the results of Gharib *et al.* (1998), they conclude that the interaction of the trailing jet instability with the leading vortex ring causes a 20% variation in vortex ring circulation, when non-dimensionalized with the orifice diameter and maximum piston velocity. We note in passing that Mohseni *et al.* (2001) showed that this variation will be diminished if the vortex ring circulation is normalized by the translational velocity and the impulse of the leading vortex ring.

While the Kelvin–Benjamin principle offers an elegant theory for the mere existence of the formation number, by itself it fails to suggest a process for the dynamics of pinch-off. On the other hand, Shusser and Gharib (2000) have shown that the Kelvin–Benjamin principle is equivalent to the hypothesis that the pinch-off occurs when the translational velocity of the ring equals the jet flow velocity near the ring. The authors

proposed a way of modelling vortex ring formation based on this kinematic approach. The purpose of the present paper is to model the formation of a vortex ring using the idea of Shusser and Gharib (2000).

The main difficulty in the theoretical analysis of the vortex ring formation stems from strong dependence of the formation number on the form of the velocity profile. In the experimental set-up, the velocity profile is determined by the motion of the piston and the geometry of the orifice or the nozzle, i.e. the velocity program, piston stroke ratio L/D and Reynolds number (Didden, 1979). Rosenfeld *et al.* (1998) reached a conclusion that experimentally found small variations in the formation number are due to different evolution of the velocity profile of the discharged flow.

Experimentally observed variations of the exit velocity profile are small and cause only slight variations in the formation number that do not detract from its universality. On the other hand, choosing a wrong approximation for this profile while modelling vortex ring formation may cause large errors in predicted formation number values. In this work we try to find a realistic approximation for the velocity profile while modelling the formation of real vortex rings. We do it by analysing boundary layer growth on the inner wall of the cylinder and its influence on the formation number. The predictions of the model can be compared with the experimental data of Gharib *et al.* (1998) and the numerical results of Rosenfeld *et al.* (1998).

The present paper is a continuation of the studies of Gharib *et al.* (1998) and Rosenfeld *et al.* (1998). Therefore, the review of previous works on vortex ring formation is not repeated here. The reader is referred to the above papers, as well as to the excellent reviews of Shariff and Leonard (1992) and Lim and Nickels (1995).

2. Boundary Layer Growth

2.1. Theoretical Model

Consider a boundary layer created at the inner surface of a cylinder of diameter D by a moving piston (see Figure 1). This boundary layer must be sufficiently thin, because otherwise the roll-up of the vortex sheet and vortex ring formation are impossible. Due to its being thin, one can neglect the influence of the nozzle wall curvature and approximate the boundary layer on the wall as a boundary layer on a semi-infinite plate. For later analysis of the impulsive piston program, we consider the growth of an unsteady boundary layer on a semi-infinite plate that at the initial moment $t = 0$ was given a constant velocity U_p .

The above problem was considered earlier (Rosenhead 1963, pp. 360–362). The solution was found to depend strongly on the parameter $\tau = U_p t/x$. For small values of τ the flow can be approximated as the Rayleigh–Stokes solution for an infinite plate, while for large τ it is closer to the Blasius solution. We mention in passing that for very large τ the assumption of a thin boundary layer becomes invalid and the flow-field can be found from the recent solution of Das and Arakeri (1998).

For constant piston velocity the parameter τ can be written as $\tau = L/x$, where L is a piston stroke ($L = U_p t$). We are interested in estimating the boundary layer thickness at the edge of the nozzle. Taking into account that in most cases $L \leq 4D$ (Gharib *et al.*, 1998) and that in Gharib *et al.*'s (1998) experiments the distance between the piston and the nozzle edge remained larger than $4D$, we obtain that $\tau < 1$ and therefore the Stokes boundary layer solution should be used.

This solution is given by Rosenhead (1963, p. 137) as

$$u = U_p \operatorname{erf} \left(\frac{y}{\sqrt{\nu t}} \right). \quad (1)$$

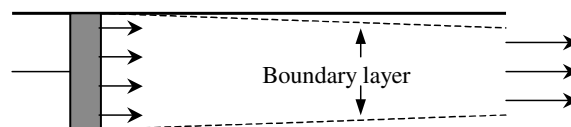


Figure 1. Boundary layer growth (not to scale) and its displacement effect during the piston motion.

Here u is the fluid velocity component parallel to the wall, y is the local coordinate normal to the wall, ν is the kinematic viscosity and

$$\operatorname{erf}(z) = \frac{2}{\sqrt{\pi}} \int_0^z e^{-\lambda^2} d\lambda. \quad (2)$$

In calculating the velocity defect, one obtains

$$\int_0^\infty (U_P - u) dy = U_P \sqrt{\frac{\nu t}{\pi}}. \quad (3)$$

Then integrating over the surface of the nozzle, we find that the presence of the boundary layer decreases the mass flow near the wall at the nozzle exit by

$$Q = U_P D \sqrt{\pi \nu t}. \quad (4)$$

To compensate for slower flow in the boundary layer the flow velocity at the nozzle exit U_{EX} must be greater than U_P . Assuming the flow outside the boundary layer is uniform and the layer itself being thin, we can write the mass conservation equation as

$$U_{\text{EX}} \frac{\pi D^2}{4} - Q = U_P \frac{\pi D^2}{4}. \quad (5)$$

Then

$$U_{\text{EX}} = U_P \left(1 + \frac{4}{\sqrt{\pi}} \frac{1}{\sqrt{Re}} \sqrt{\frac{L}{D}} \right). \quad (6)$$

Here $Re = U_P D / \nu$.

We now verify the accuracy of the theoretical result by calculating numerically a piston-driven flow in the cylinder.

2.2. Numerical Model

The axisymmetric time-dependent incompressible Navier–Stokes equations in dimensionless form are employed for simulating the unsteady flow in the tube:

$$\begin{aligned} \frac{\partial u_r}{\partial t} + u_r \frac{\partial u_r}{\partial r} + u_x \frac{\partial u_r}{\partial x} &= \frac{1}{r} \frac{\partial}{\partial r} (r \sigma_{rr}) - \frac{1}{r} \sigma_{\theta\theta} + \frac{\partial \sigma_{rx}}{\partial x}, \\ \frac{\partial u_x}{\partial t} + u_r \frac{\partial u_x}{\partial r} + u_x \frac{\partial u_x}{\partial x} &= \frac{1}{r} \frac{\partial}{\partial r} (r \sigma_{rx}) + \frac{\partial \sigma_{xx}}{\partial x}, \\ \frac{1}{r} \frac{\partial}{\partial r} (r u_r) + \frac{\partial u_x}{\partial x} &= 0. \end{aligned} \quad (7)$$

The stress components are given by

$$\begin{aligned} \sigma_{rr} &= -P + \frac{2}{Re} \frac{\partial u_r}{\partial r}, & \sigma_{\theta\theta} &= \frac{2}{Re} \frac{u_r}{r}, \\ \sigma_{rz} &= \frac{1}{Re} \left(\frac{\partial u_r}{\partial x} + \frac{\partial u_x}{\partial r} \right), & \sigma_{zz} &= -P + \frac{2}{Re} \frac{\partial u_x}{\partial x}. \end{aligned} \quad (8)$$

The velocity components in the axial (x) and radial (r) directions are u_x and u_r , respectively, and P is the pressure.

It should be noted that for a very long pipe and a sufficiently high Reynolds number the assumption of axisymmetric flow becomes invalid. However, this fact has no influence on vortex ring formation because in practice vortex ring pinches off long before that. Gharib *et al.* (1998) were especially interested in long piston strokes. They observed that the flow remained axisymmetric with a good accuracy. Even Glezer and

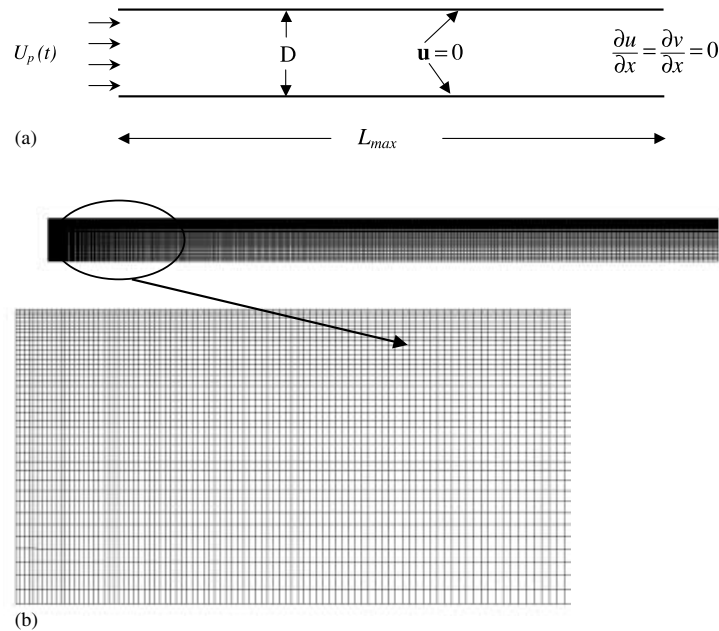


Figure 2. The computational domain and boundary conditions used in the starting flow in a pipe: (a) computational domain; (b) the mesh used (for clarity purposes, only every other mesh point is shown in each direction).

Coles (1990), who studied turbulent vortex ring formation and used piston velocities that were about an order of magnitude higher than those used by Gharib *et al.* (1998), observed an axisymmetric flow. Das and Arakeri (1998), who investigated transition in a piston-driven pipe flow for piston strokes as large as 28 pipe diameters, state explicitly (p. 257) that the flow remained unidirectional for a considerable time.

The computational domains and the boundary conditions are shown in Figure 2(a). The flow is solved inside a tube of diameter 2.5 cm and length 20 cm. In the inflow boundary, a uniform axial flow with a magnitude of 8 cm/s was specified, which corresponds to a Reynolds number (based on the tube diameter and the inflow velocity) of 2000 for water flow. On the tube, zero velocity is specified, while on the outlet, zero gradient is imposed on the velocity. Zero velocity was assumed as the initial conditions. A commercial CFD solver (FLUENT 5, Fluent Inc., Lebanon, New Hampshire) was employed to solve numerically the Navier–Stokes equations. The PISO method was used for pressure–velocity coupling. Second-order temporal and spatial schemes were used for obtaining accurate predictions.

A mesh of 81×641 nodes was used in the radial and axial directions, respectively (see Figure 2(b)). Mesh points were clustered near the wall and in the vicinity of the upstream boundary, where the largest gradients were found. A uniform time step of $\Delta t = 0.002$ s was used to advance the solution in time; it corresponds to a non-dimensional time step of $\Delta t^* = U_P \Delta t / D = 0.0064$, i.e. more than 150 time steps for every stroke of one diameter. Mesh and time-step refinement tests revealed that the mesh and time steps used in the present numerical simulations are within the convergence zone.

2.3. Results

The axial velocity distribution for several instants is shown in Figure 3. The flow-field is dominated by two regions: the Stokes boundary layer region and the time-dependent spatially developing region.

In Figure 3(a), one finds a large region of spatially uniform velocity as well as a thin Stokes layer near the wall and a developing flow in a small entrance region. In the later times, the developing flow region is propagating downstream, constantly resulting in the reduction of the Stokes flow region. A clear front can be observed between the developing flow and the Stokes flow. For example, in Figure 3(b) the front is at the most downstream vertical line.

Figure 4 shows the axial velocity component on the axis at the time of $t = 0.65$ s. Both flow regions can be observed here as well. For $x < 0.05$ m ($x/D < 2$) the flow is spatially developing and increasing in

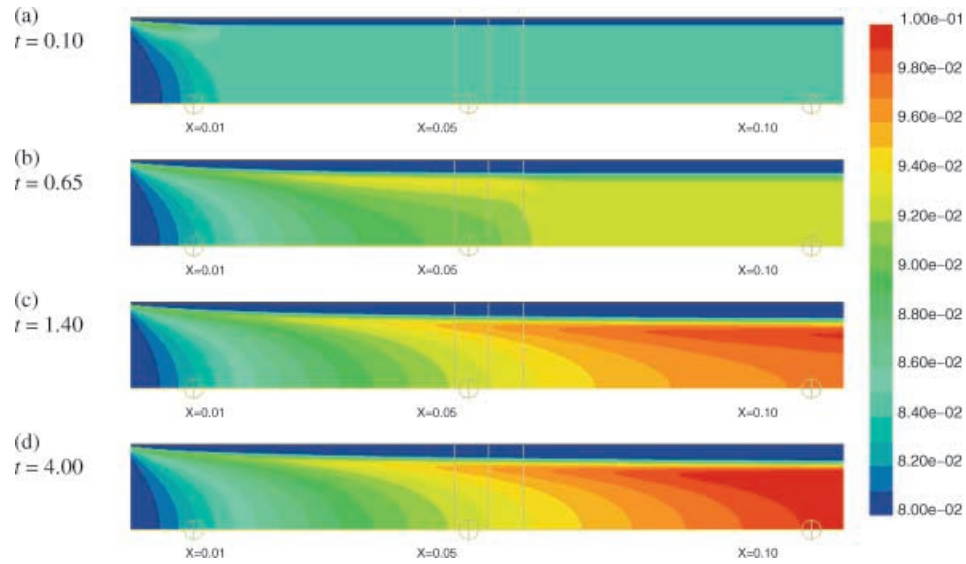


Figure 3. The axial velocity distribution evolution in time for starting flow in a pipe. The small circles mark the points along which time history is shown in Figure 7. The vertical lines mark location of the lines along which the axial velocity distribution is shown in Figure 5: (a) $t = 0.10$ s; (b) $t = 0.65$ s; (c) $t = 1.40$ s; (d) $t = 4.00$ s.

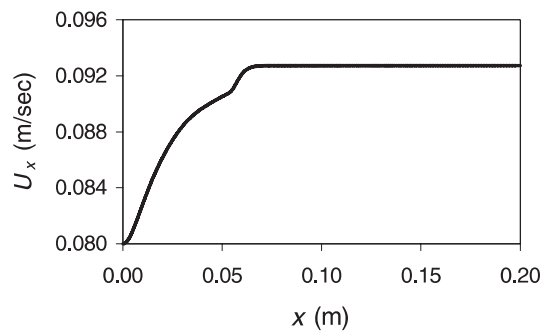


Figure 4. The axial velocity on the axis for $t = 0.65$ s.

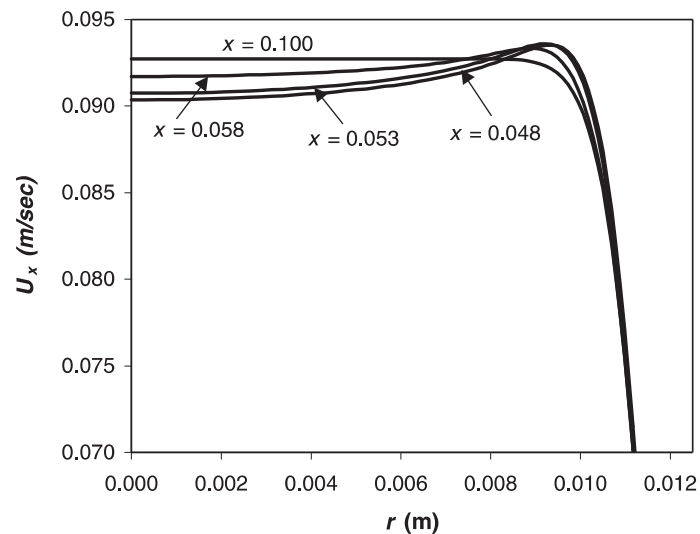


Figure 5. The axial velocity profile at several axial locations and $t = 0.65$ s.

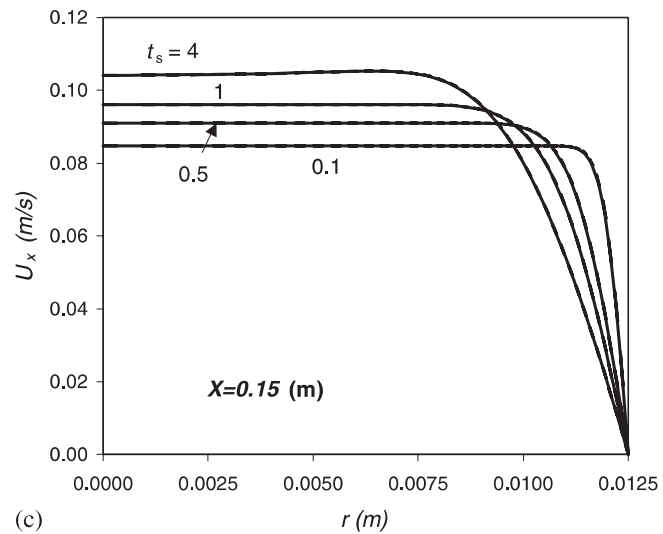
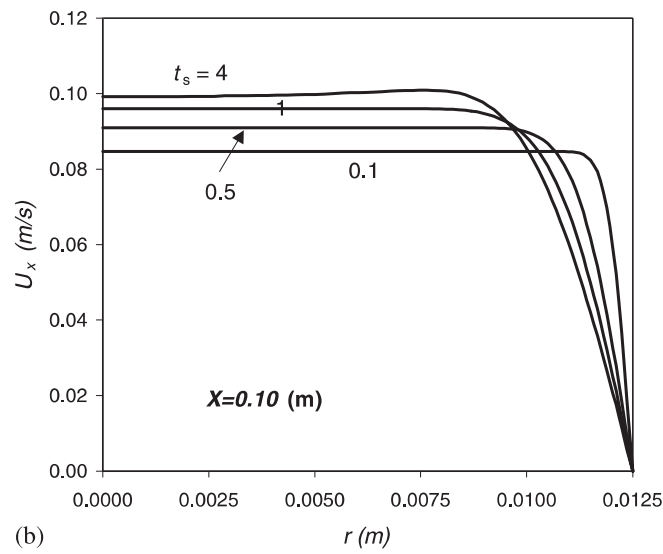
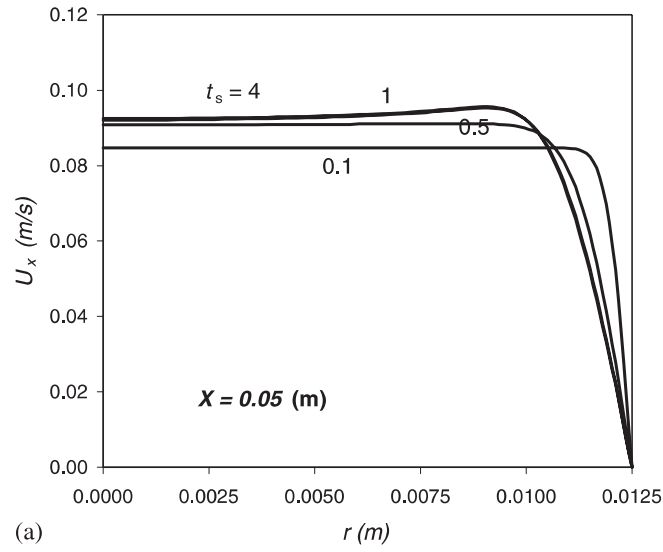


Figure 6. The axial velocity profile at several axial cross-sections: (a) $x = 0.05$ m; (b) $x = 0.1$ m; (c) $x = 0.15$ m.

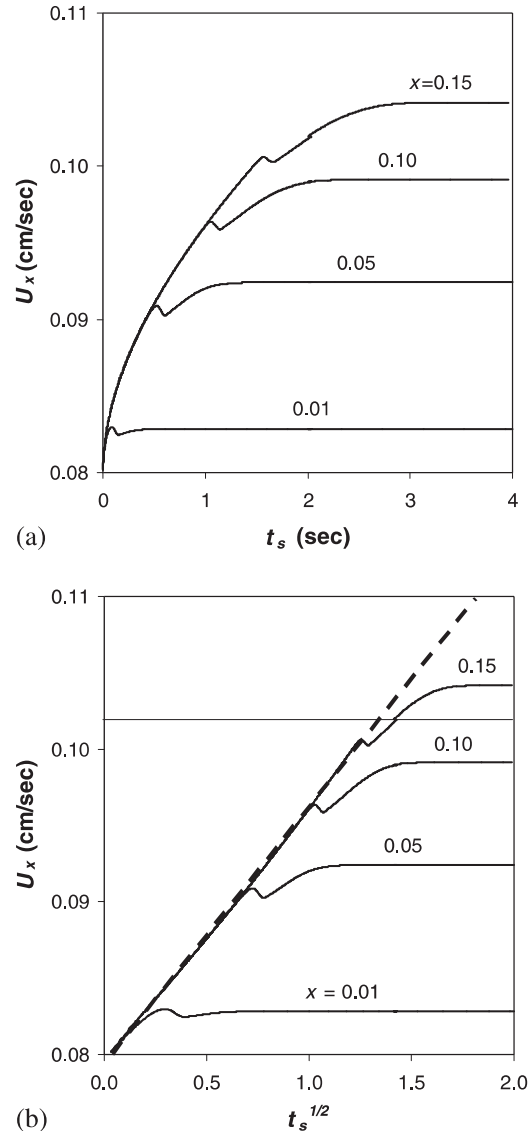


Figure 7. Axial velocity history at four points on the axis: (a) as a function of t ; (b) as a function of \sqrt{t} .

magnitude, while for $x > 0.06$ m the velocity on the axis is uniform. The axial velocity profile at that time ($t = 0.65$ s) is shown in Figure 5 at four axial locations, three of which are marked by the vertical lines in Figure 3. Far downstream ($x = 0.1$ m, i.e. $x/D = 4$) the flow-field consists of a Stokes boundary layer with a large uniform core region. At $x < 0.58$ m, the velocity profile is typical of the initial stages of a developing flow. An “overshoot” in the velocity is found near the wall and consequently the velocity on the axis is smaller than its maximum value in the Stokes layer region. The latter phenomenon was observed experimentally by Didden (1979).

The time evolution of the axial velocity profile at three axial sections (see their location in Figure 3) is shown in Figure 6. The previous findings are supported in this figure as well.

The history of the axial velocity at four points on the axis, which are also marked in Figure 3 by the crossed dots, is shown in Figure 7(a). The initial stage is characterized by the Stokes layer, while the later stages exhibit spatially developing flow characteristics. There is a noticeable decrease in the axial velocity when the developing flow front passes, i.e. the axis line velocity decreases in the developing flow region. Figure 7(b) depicts the same data as a function of \sqrt{t} demonstrating the Stokes layer behaviour prior to the passing of the developing flow front.

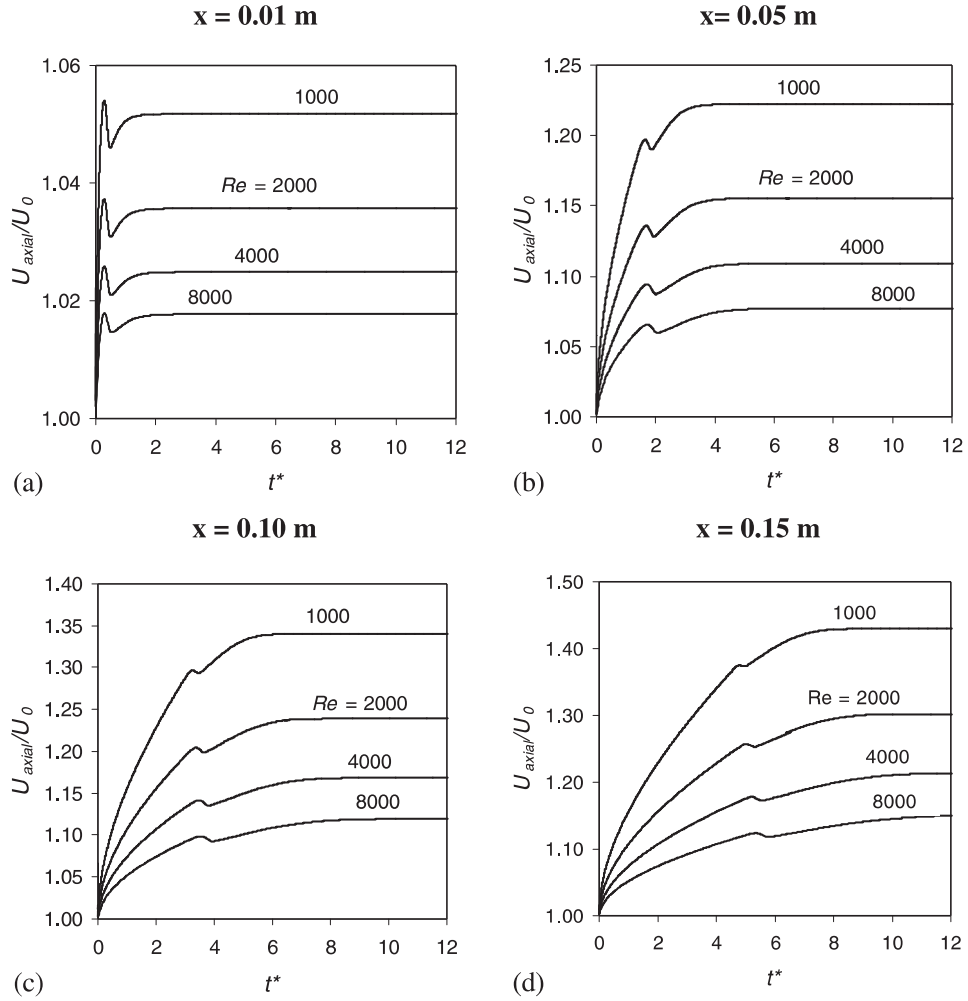


Figure 8. The dependence of the centreline velocity on the Reynolds number at several axial locations: (a) $x = 0.01$ m; (b) $x = 0.05$ m; (c) $x = 0.10$ m; (d) $x = 0.15$ m.

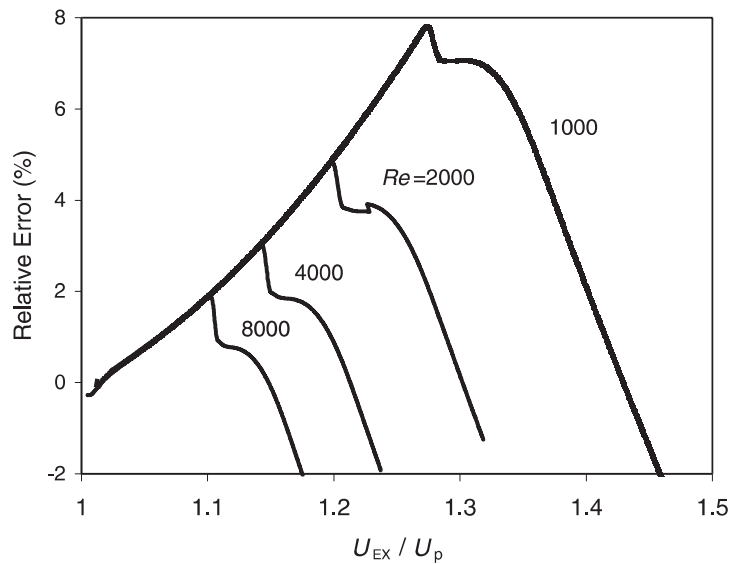


Figure 9. The relative error for (6) as a percentage at $x = 0.15$ m.

To study the influence of the Reynolds number, we repeated the calculations for inflow velocities U_0 of 4 cm/s, 16 cm/s and 32 cm/s, which correspond to Reynolds numbers of 1000, 4000 and 8000, respectively.

Figure 8 shows the dependence of the axial velocity U_{axial} at four axial locations as a function of dimensionless time $t^* = U_0 t / D$. We see that though the increase in the Reynolds number from 1000 to 8000 causes a difference of about 25% in the values of the scaled axial velocity $U_c = U_{\text{axial}} / U_0$ (see Figure 8(d)), the form of the time evolution remains the same for all Reynolds numbers.

To verify the validity of the theoretical model of Section 2.1, we plotted on Figure 9 the relative error for the cross-section $x = 0.15$. The relative error was defined as $(U_c - U_{\text{EX}}) / U_{\text{EX}}$, where U_{EX} is given in (6). One sees that the error does not exceed 8% and that for $Re \geq 2000$ it remains less than 5%.

Summing up, we can conclude that the velocity profile at the exit of the tube is that of a Stokes layer in a straight pipe with a peak in the axial velocity near the wall. The agreement between the theory and the numerical calculations is quite acceptable. We now use the boundary layer correction (6) to improve the slug-flow approximation while modelling the vortex ring formation.

3. Vortex Ring Formation

3.1. Formation Model

Consider formation of a laminar vortex ring in a piston/cylinder arrangement. In order to concentrate on the main physical factors, we study the basic case of a constant piston velocity U_P (an impulsive velocity program).

For convenience, we briefly summarize the main points of the vortex ring formation model proposed by Shusser and Gharib (2000).

Vortex ring formation in a piston/cylinder arrangement is caused by roll-up of a cylindrical vortex sheet ejected from the cylinder. The pinch-off occurs when vorticity flux from the vortex sheet into the ring vanishes. Assuming a uniform velocity across the ring-generating jet and calculating the vorticity flux, one can show that the pinch-off criterion is

$$W = V_{\text{jet}}, \quad (9)$$

where W is the translational velocity of the vortex ring and V_{jet} is the flow velocity of its generating jet near the vortex ring. Details are given in the Appendix.

Shusser and Gharib (2000) assumed that in the vicinity of the ring the radius of the generating jet is equal to the vortex ring radius R . Then using conservation of mass one can relate V_{jet} to the piston velocity U_P :

$$V_{\text{jet}} = \frac{U_P D^2}{4R^2}. \quad (10)$$

Substituting (10) into (9), one obtains Shusser and Gharib's (2000) pinch-off criterion

$$W = \frac{U_P D^2}{4R^2}. \quad (11)$$

To calculate the translational velocity of the vortex ring W and its radius R , Shusser and Gharib (2000) adopted the approach of Mohseni and Gharib (1998) and approximated the ring as a member of Norbury's family of vortex rings (Norbury, 1973). Each particular member of Norbury's family is characterized by the non-dimensional thickness of the ring core ε , which varies between zero and $\sqrt{2}$.

Using Norbury's family for vortex ring modelling one assumes that the vortex ring created in the laboratory will have the same relationships between its impulse, energy and translational velocity as a member of Norbury's family. (The extent to which the normalized circulation and energy of the computed vortex rings are consistent with the mean core radius, as defined by Norbury, was investigated by Mohseni *et al.* (2001).) However, these relationships depend on the thickness of Norbury's ring ε .

To calculate the energy, impulse and circulation of the vortex ring, Shusser and Gharib (2000) used the slug-flow approximation (Shariff and Leonard, 1992; Lim and Nickels, 1995):

$$E = \frac{1}{8}\pi D^2 \rho L U_P^2, \tag{12}$$

$$I = \frac{1}{4}\pi D^2 \rho L U_P, \tag{13}$$

$$\Gamma = \frac{1}{2} L U_P. \tag{14}$$

Here E is the vortex ring energy, I is the vortex ring impulse, Γ is the vortex ring circulation and ρ is the density of the fluid. The following relationships can be obtained from (12)–(14):

$$E = \frac{IU_P}{2}, \tag{15}$$

$$I = \frac{\pi D^2 \rho}{2} \Gamma. \tag{16}$$

One can use (11), (15) and (16) to derive the following equation for the vortex ring thickness at pinch-off:

$$\alpha(\varepsilon) = \frac{B(\varepsilon)}{2N(\varepsilon)\sqrt{\pi}}. \tag{17}$$

Here

$$\alpha = \frac{E}{\sqrt{\rho I \Gamma^3}}, \tag{18}$$

$$B = W \sqrt{\frac{\pi I}{\rho \Gamma^3}}, \tag{19}$$

$$b = R \sqrt{\frac{\rho \pi \Gamma}{2I}}, \tag{20}$$

$$N = \frac{W}{U_P}. \tag{21}$$

It should be noted that, for Norbury’s family, α , B , b and N are functions of the non-dimensional thickness ε only.

Shusser and Gharib (2000) suggested using (17) to estimate the value of ε . Using Tables 1 and 2 of Norbury (1973), one can calculate α , B , b and N for seven values of ε between 0.2 and $\sqrt{2}$. The results are shown in Table 1.

One sees from Table 1 that (17) does have a solution. Unfortunately, it is not possible to calculate it exactly due to the absence of data for intermediate values of ε . Nevertheless, it is clear that the root of (17) corresponds to ε that is slightly more than 0.4. For example, an interpolation of the data from Table 1 by a polynomial of order 4 or higher or by cubic splines yields $\varepsilon \approx 0.44$.

We therefore approximate the vortex ring as a Norbury ring with a thickness of $\varepsilon = 0.4$. Incidentally, this is the average value of what one obtains by matching the translational velocity of the vortex ring ($\varepsilon \approx 0.3$, Mohseni and Gharib (1998)) and by matching its energy ($\varepsilon \approx 0.5$, Shusser and Gharib (2000)). We also consider the sensitivity of the results to variation in ε later.

Table 1. Calculation of α , B , b , N from Norbury’s (1973) data.

ε	0.2	0.4	0.6	0.8	1.0	1.2	$\sqrt{2}$
α	0.5567	0.3640	0.2754	0.2214	0.1873	0.1666	0.1601
B	0.8610	0.6907	0.5876	0.5119	0.4553	0.4162	0.3974
b	0.6978	0.6775	0.6558	0.6356	0.6153	0.5921	0.5590
N	0.5135	0.5446	0.5814	0.6188	0.6604	0.7132	0.8
$B/2N\sqrt{\pi}$	0.4730	0.3578	0.2851	0.2334	0.1945	0.1646	0.1401

For the basic case of the uniform velocity profile and constant velocity program, criterion (11) yields the following result for the formation number:

$$\frac{L}{D} = \frac{\pi\sqrt{2}}{4b^2B}. \quad (22)$$

For a Norbury ring with $\varepsilon = 0.4$, $B = 0.6907$ and $b = 0.6775$ (see Table 1). Hence $L/D = 3.50$.

This is very close to Rosenfeld *et al.*'s (1998) result for the case of a uniform velocity profile and an impulsive velocity program ($L/D = 3.60$). One sees that even for the idealized case of a uniform velocity profile, our prediction is very close to the numerical results. However, to obtain experimental values of the formation number, the model should account for boundary layer growth and its influence on the exit velocity profile.

As the data for Norbury's vortices is given in Norbury (1973) only in table format, its direct use is not very convenient in practice. To facilitate calculating vortex ring properties, we utilize Fraenkel's second-order formulae for Norbury's vortices (Fraenkel, 1972):

$$B(\varepsilon) = \frac{1}{4}\sqrt{1 + \frac{3}{4}\varepsilon^2} \left[\ln \frac{8}{\varepsilon} - \frac{1}{4} + \frac{3\varepsilon^2}{8} \left(\frac{5}{4} - \ln \frac{8}{\varepsilon} \right) \right], \quad (23)$$

$$b(\varepsilon) = \frac{1}{\sqrt{2(1 + \frac{3}{4}\varepsilon^2)}}. \quad (24)$$

For $\varepsilon = 0.4$, (22)–(24) yield $B = 0.6987$, $b = 0.6682$ and $L/D = 3.56$. One sees that the difference between Norbury's data and Fraenkel's approximation is very small, as the error is 1.2% for B , 1.4% for b and 1.7% for the formation number. We can conclude that the accuracy of Frankel's formulae is good.

3.2. Boundary Layer Correction

We now use a more realistic approximation (6) accounting for the boundary layer correction to the flow velocity in the ring-generating jet. Therefore, instead of (11) our criterion for the pinch-off will be

$$W = \frac{U_{EX}D^2}{4R^2}. \quad (25)$$

Substituting (6) into (25) and using (13)–(14), (19)–(20), we obtain a quadratic equation for the formation number L/D :

$$\frac{L}{D} - \frac{\sqrt{2\pi}}{b^2B} \frac{1}{\sqrt{Re}} \sqrt{\frac{L}{D}} - \frac{\pi\sqrt{2}}{4b^2B} = 0. \quad (26)$$

Taking the positive root one finally arrives at

$$\frac{L}{D} = \frac{\pi}{2B^2b^4Re} \left[1 + \sqrt{1 + \frac{ReBb^2}{\sqrt{2}}} \right]^2. \quad (27)$$

The relationship (27) for three values of ε is plotted in Figure 10, where the numerical results of Rosenfeld *et al.* (1998) are also shown. We see that two other values of ε do not give good results. The predicted formation number values are too low for $\varepsilon = 0.3$ and too high for $\varepsilon = 0.5$.

For $\varepsilon = 0.4$, one sees that owing to the boundary layer correction the values of the formation number now lie in the range 3.8–4, which is exactly what was found experimentally by Gharib *et al.* (1998). When the Reynolds number is large, the model predictions are in very good agreement with the numerical calculations.

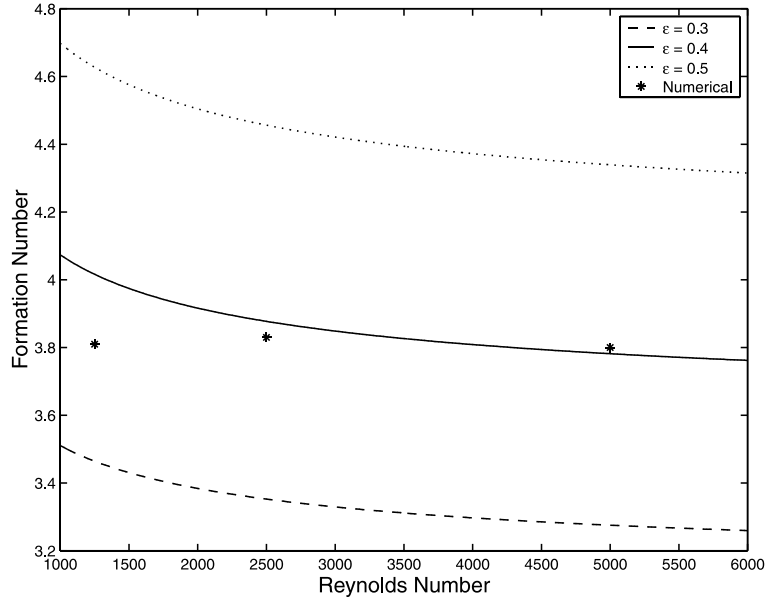


Figure 10. The dependence of the formation number on the Reynolds number: comparison of theoretical and numerical results.

The error is 0.5% for $Re = 5000$ and 1.3% for $Re = 2500$. For smaller Reynolds numbers, the accuracy of the predicted formation time decreases somewhat due to larger relative errors in the boundary layer approximation we used in Section 2 (see Figure 9). Nevertheless, even for low Reynolds number values such as $Re = 1250$, the model provides an acceptable accuracy of 5.5%. This means that the model predictions are reliable for the whole range of Reynolds numbers corresponding to laminar vortex ring formation.

4. Conclusions

We have proposed a new improved model for laminar vortex ring formation in a piston/cylinder arrangement that accounts for the boundary layer growth on the cylinder wall. Numerical calculation of a developing boundary layer in a piston-driven pipe flow demonstrates that the Stokes layer generated by an impulsively started flat plate is an adequate model of the boundary layer. Predicted formation number values now fall in the experimentally observed regime.

5. Appendix. Physical Basis for Shusser and Gharib's (2000) Pinch-Off Criterion

The ring is formed by the roll-up of a cylindrical vortex sheet emitted from the pipe. Hence the ring will pinch off when the flux of vorticity from the vortex sheet into the ring vanishes.

Due to the vortex sheet being thin, using the boundary layer approximation one can show that the vorticity flux across the cross-section of the sheet is (Lim and Nickels, 1995, p. 115)

$$\int \omega_{\theta} u \, dr \approx \int \frac{\partial u}{\partial r} u \, dr = \frac{1}{2} V_{\text{jet}}^2. \quad (\text{A.1})$$

Here ω_{θ} is the azimuthal vorticity, u is the axial velocity inside the sheet, r is the radial coordinate and the integration is taken across the sheet. It is assumed in (A.1) that the velocity at the inner edge of the sheet is equal to the flow velocity in the ring-generating jet, V_{jet} . This assumption is equivalent to postulating a uniform velocity across the jet.

On the other hand, not all the flux (A.1) will reach the ring. This will happen only for those parts of the sheet where the local axial velocity u is larger than the translational velocity of the ring W . Assuming that u

increases monotonically across the sheet from $V_{\text{out}} < W$ to $V_{\text{jet}} > W$, we obtain for the vorticity flux into the ring

$$\int_{u>W} \omega_{\theta}(u - W) dr \approx \int_{u>W} \frac{\partial u}{\partial r}(u - W) dr = \frac{1}{2}(V_{\text{jet}} - W)^2. \quad (\text{A.2})$$

One sees that the flux (A.2) vanishes and the ring pinches off from its generating jet when the translational velocity of the ring equals the jet flow velocity near the ring.

References

- Amick, C.J., and Fraenkel, L.E. (1986). The uniqueness of Hill's spherical vortex. *Arch. Rational Mech. Anal.*, **92**, 91–119.
- Benjamin, T.B. (1976). The alliance of practical and analytical insights into the non-linear problems of fluid mechanics. In *Application of Methods of Functional Analysis to Problems in Mechanics* (P. Germain and B. Nayroles eds.) pp. 8–28, Lecture Notes in Mathematics, vol. 503. Springer-Verlag, Berlin.
- Das, D., and Arakeri, J.H. (1998). Transition of unsteady velocity profiles with reverse flow. *J. Fluid Mech.*, **374**, 251–283.
- Didden, N. (1979). On the formation of vortex rings: rolling-up and production of circulation. *Z. Angew. Math. Phys.*, **30**, 101–116.
- Fraenkel, L.E. (1972). Examples of steady vortex rings of small cross-section in an ideal fluid. *J. Fluid Mech.*, **51**, 119–135.
- Friedman, A., and Turkington, B. (1981). Vortex rings existence and asymptotic estimates. *Trans. Am. Math. Soc.*, **268**, 1–37.
- Gharib, M., Rambod, E., and Shariff, K. (1998). A universal time scale for vortex ring formation. *J. Fluid Mech.*, **360**, 121–140.
- Glezer, A., and Coles, D. (1990). An experimental study of a turbulent vortex ring. *J. Fluid Mech.*, **211**, 243–283.
- Kelvin, Lord (1880). Vortex statics. *Philos. Mag.*, Ser. 5, **10**, 97–109.
- Lim, T.T., and Nickels, T.B. (1995). Vortex rings. In *Fluid Vortices* (S.I. Green ed.), pp. 95–153, Kluwer, Dordrecht.
- Mohseni, K. (2001). Statistical equilibrium theory of axisymmetric flows: Kelvin's variational principle and an explanation for the vortex ring pinch-off process. *Phys. Fluids*, **13**(7), 1924–1931.
- Mohseni, K., and Gharib, M. (1998). A model for universal time scale of vortex ring formation. *Phys. Fluids*, **10**(10), 2436–2438.
- Mohseni, K., Ran, H., and Colonius, T. (2001). Numerical experiments on vortex ring formation. *J. Fluid Mech.*, **430**, 267–282.
- Norbury, J. (1973). A family of steady vortex rings. *J. Fluid Mech.*, **57**, 417–431.
- Rosenfeld, M., Rambod, E., and Gharib, M. (1998). Circulation and formation number of laminar vortex rings. *J. Fluid Mech.*, **376**, 297–318.
- Rosenhead, L. (1963). *Laminar Boundary Layers*. Clarendon Press, Oxford.
- Shariff, K., and Leonard, A. (1992). Vortex rings. *Annu. Rev. Fluid Mech.*, **24**, 235–279.
- Shusser, M., and Gharib, M. (2000). Energy and velocity of a forming vortex ring. *Phys. Fluids*, **12**(3), 618–621.
- Wan, Y.-H. (1988). Variational principles for Hill's spherical vortex and nearly spherical vortices. *Trans. Am. Math. Soc.*, **308**, 299–312.
- Zhao, W., Frankel, S.H., and Mongeau, L.G. (2000). Effects of trailing jet instability on vortex ring formation. *Phys. Fluids*, **12**(3), 589–596.